Photosensitization of Nanostructured TiO_2 with WS_2 Quantum Sheets

Markus Thomalla* and Helmut Tributsch

Hahn Meitner Institut, Department Solare Energetik, 14109 Berlin, Germany

Received: March 6, 2006; In Final Form: March 22, 2006

Porous, nanostructured sol gel TiO_2 (100 nm) has been sensitized with WS_2 quantum sheets (∼5 nm) with the help of chemical bath deposition. The absorber has been characterized with help of energy dispersive X-ray (EDX), transmission electron microscopy (TEM), scanning electron microscopy (SEM), Raman spectroscopy, and light absorption measurements. The photosensitization was confirmed via electrochemical measurements. The surface of TiO_2 has been modified by a thin Al_2O_3 film, which significantly enhanced the photocurrent density to 0.4−0.7 mA/cm^2. Moiré patterns suggest that the S−W−S layers of WS_2 are not perfectly aligned in the direction of the *c*-axis, emphasizing the role of lateral electron transfer, which is also evidenced by surface passivation experiments. With WS_2, a new, cheap, environmentally friendly, and stable absorber material for the sensitization of wide band gap nanomaterials has been introduced.

Introduction

Nanostructured photo-electrochemical solar cells have received considerable attention in recent years as an alternative to conventional solar cells. In particular, the solar cell developed by Grätzel and his group with its high solar energy conversion of up to 11% has increased the research efforts in this field.[1] Unfortunately, the original *cis*-$RuL_2(SCN)_2$ with L = 2,2′-bipyridyl-4,4′-dicarboxylatoacid (bpca) dye does not have the desirable stability of 20 years,[2−5] and in addition to the iodine redox system, the volatile solvent and its confinement provide problems. An interesting approach is to replace the organic dye with an inorganic semiconductor quantum dot. Semiconductor quantum dots have several advantages. First, their band gap can be easily adjusted by changing the size of the particle to match the solar spectrum and the band gap of TiO_2. Second, they may be selected to possess a high absorption coefficient, which allows one to produce a very thin absorber and to reduce the amount of materials needed. And most important, it may be possible to apply a metallically conducting nanocontact as they are used in traditional solid state solar cells.

Several research groups have already tried to sensitize the TiO_2 with inorganic materials such as CdSe,[6−8] CdS, PbS, Ag_2S, Sb_2S_3, and Bi_2S_3,[9,10] In_2S_3,[11] and RuS_2.[12]

In our work, we used for the first time WS_2, a very stable and potentially cheap semiconductor. Its stability is due to the photoexcitacion of d-orbital electrons which do not participate in essential chemical bonding. Colloids have therefore proved to be photo stable.[13] The issue of photostability of colloids appears to be very important, because nanoparticles in which electron exitation may break chemical bonds such as CdSe, CdS, and PbS may rapidly degrade. Another advantage of WS_2 is that it is not poisonous or hazardous for the environment. Molybdenum and tungsten dichalcogenides crystals have demonstrated high energy conversion efficiency in electrochemical solar cells (more than 15%), and they have reached 7−8% in preliminary experiments toward solid-state solar cells.[14] Their indirect band gap is around 1.34 eV [15,16] and matches well the sun spectrum. However, it is well-known that step sites and surfaces perpendicular to the *c*-axis pose major problems as recombination centers for photogenerated charges. Many efforts have therefore been undertaken to chemically passivate such surface sites by chemical modification or attachment of molecular species.[17−25] A nanosolar cell based on WS_2 will therefore necessarily include efforts toward chemical passivation of such undesirable properties on the nanoscale.

Experimental Procedures

The TiO_2 layers produced via the sol gel method on a conducting substrate (fluorine doped glass, 15 Ω/cm^2) were purchased from SGLux. Prior to CBD, all samples were heated to 150 °C to remove the water residues from TiO_2 pores.

The porous TiO_2 has been sensitized via the chemical bath deposition (CBD) technique.[26] First, pure S (all chemicals, if not otherwise stated, were purchased from Fluka) has been dissolved in 50 mL cymene (1-isopropyl-4-methylbenzene, $CH_3C_6H_4CH(CH_3)_2$) to obtain a 0.1 M solution. Then, the TiO_2 samples were carefully put into the glass container with the sulfur solution and placed at 45° inclined to the vertical wall with the TiO_2 side oriented toward the bottom. Then, the solution was heated to 170 °C until the boiling point was reached. After 20 min (to allow the dissolved sulfur to penetrate the TiO_2 pores), $W(CO)_6$ was added to obtain a 0.05 M solution and then the top of the container was covered with a glass top. Immediately, the color of the solution changed to dark brown. After waiting for an additional 30 s to 2 min, the substrates were removed from the container and dried in air. Then, they were washed with acetone and dest. water and put into a vacuum to remove the rest of the organic solvent. Other solvents instead of cymene (boiling point 178 °C) were tried, to vary the temperature of CBD such as biphenyl (255 °C), diphenylamine (302 °C), pyrene (393 °C), and naphthaline (218 °C). None of them gave better photocurrents than cymene.

The electrodes were contacted with the help of Elecolit Panasol 353, a two compound silver epoxy glue. A small part of sensitized TiO_2 was removed from the electrode. Then, the conducting glue was placed on the conducting glass with a piece of copper wire and allowed to dry.

* Corresponding author. Phone: +49 30 80622508. Fax: +49 30 80622434. E-mail: thomalla@hmi.de.

10.1021/jp061371q CCC: $33.50
Published on Web 05/27/2006

The electrodes were carefully sealed with Screentec RTV silicon rubber to avoid short circuits between the front electrode (FTO) and the liquid electrolyte.

All scanning electron microscopy (SEM) images were taken using LEO 1530 scanning electron microscope at 2 kV equipped by an energy dispersive X-ray (EDX) fluorescence analyzer to quantify the composition of the sample.

The microstructure of the films was observed by transmission electron microscopy (TEM) using a Philips CM12, and the local compositions were analyzed using an energy dispersive X-ray spectroscopy system within the TEM. For the TEM analysis, the sample was subsequently thinned by Ar ion milling.

Raman spectra were measured by a Dilor MikroRaman Labram spectrometer at room temperature. For excitation the 632.8 nm red line of He−Ne, laser was used. The detector was a Si−CCD. The accumulation time varied between 600 and 3600 s. This long accumulation time was necessary because we used filters to decrease the intensity of the laser (which was approximately 70 μW) in order not to heat up the samples. The references were crystals produced with vapor transport and controlled with X-ray diffraction (XRD) to obtain the right composition.

All absorption spectra were measured with the help of a Cary UV−vis spectrometer using a scattered light collection device (Ulbricht's sphere).

For the electrochemical measurements, a three electrode setup was used. The counter electrode was a platinum wire, and the reference electrode was an SCE (saturated calomel electrode). We used a potentiostat and a lock-in amplifier. The chopper frequency was 60 Hz. The nanostructured TiO_2 electrode has been illuminated from the front (which means from the FTO/TiO_2 side, which is the usual DSSC set up). The electrolyte used for electrochemical measurements was 0.5 M LiI dissolved in propylene carbonate (instead of the usual acetonitrile, which is poisonous). The electrolytic contact was just used for testing the photoelectrical quality of the layers, since the final aim is to develop an all solid nanostructured cell.

For Sc_2O_3 and Yt_2O_3 and ZnO barrier layers, commercial nitric acid solutions of Yt_2O_3 and Sc_2O_3 and ZnO were used as precursors. For Al_2O_3 layer, we used a solution of *tert*-butyl aluminum in dry 2-propanol. For MgO, we used magnesium-methoxide as a solution. The substrates were heated to 150 °C, then dipped into the metal solutions, dried in air, and annealed at 450 °C in air. For comparison, we always made a reference sample which was treated the same way without dipping it into the organic solution.

For chemical treatment and edge site passivation of the samples, we used a 1% TWEEN 80 (poly(ethylene glycol) sorbitan monooleate) solution in H_2O dest.

Results

Figure 1 displays the SEM micrograph of a TiO_2 cross section. The average diameter of the particles and pores is about 50−100 nm. The WS_2 material generated through the chemical reaction process was observed to penetrate the whole TiO_2 matrix to the front electrode (FTO). The color of the TiO_2 matrix was clearly seen to change from white to dark brown. It could be seen from both sides, also through the front glass, which indicates that the chemical deposition treatment had affected the entire layer. Since one could not clearly identify WS_2 particles in the SEM image with a resolution higher than 20 nm, it was concluded that the WS_2 is in form of thin quantum sheets covering the TiO_2 particles. This conclusion was supported by a simple estimation. Assuming that WS_2 is evenly

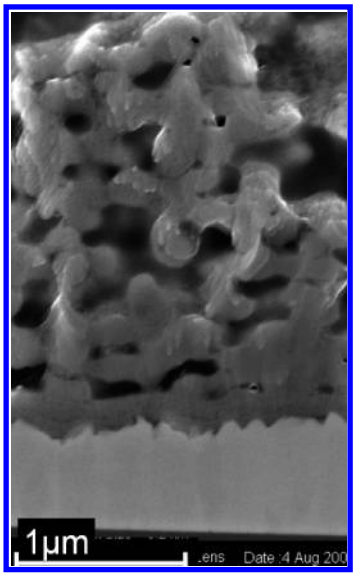

Figure 1. SEM cross section of a TiO_2 nanolayer.

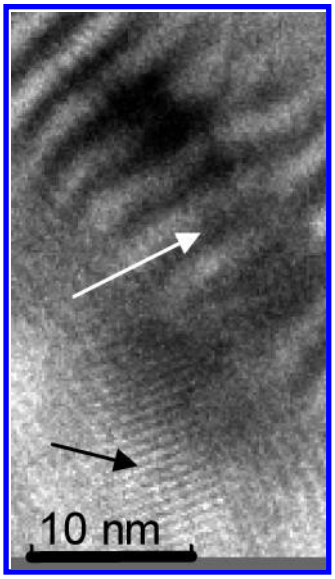

Figure 2. High-resolution TEM measurement showing TiO_2 particle structure and Moiré pattern.

distributed throughout the TiO_2 nanolayer, one could measure, on the basis of its absorption coefficient, its effective cumulative layer thickness. Considering the number of TiO_2 particles covered with WS_2 on both sides, the nominal thickness of individual layers on TiO_2 particles could be estimated to 3.5 nm. This is in agreement with the conclusion that the layered WS_2 is present in the form of layered quantum sheets. TEM measurements agree with this conclusion (Figure 2).

At the bottom of the picture, one can see the typical layered structure of WS_2 with an average layer distance of 0.75 nm (black arrow), which is slightly more than that reported in the literature (0.65−0.68 nm).[27] At the top of the picture, larger periodic patterns are observed, which could be identified as Moiré patterns. They arise from a stacking of layers in which successive layers deviate in their crystalline position.[28] It can therefore be concluded that WS_2 is present in the form of sheets which are loosely and not perfectly arranged in the direction of the *c*-axis.

It is suggested that WS_2 is deposited in the porous TiO_2 matrix as is shown in Figure 3. When the light creates an electron−hole pair, the electron is injected into the TiO_2 and moves through the network toward the front contact. The hole moves

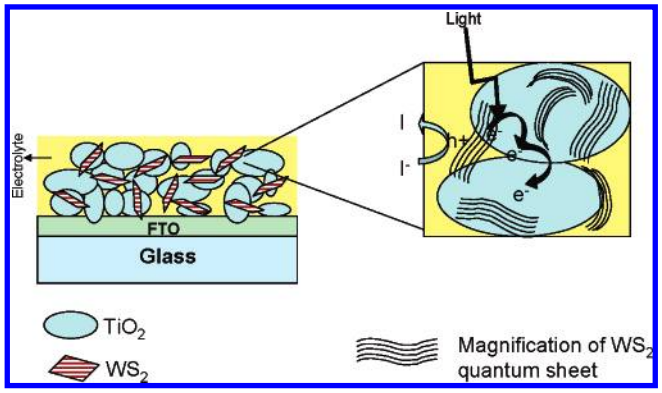

Figure 3. TiO_2 sensitized with WS_2, magnification (right).

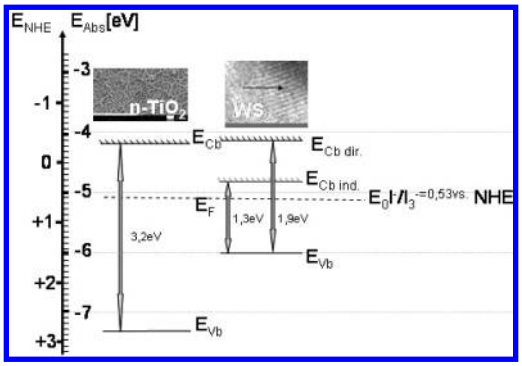

Figure 4. Energy scheme for WS_2 interacting with TiO_2: (right) redox potential of the electrolyte; (E_{Cbdir}) direct band gap; (E_{Cbind}) indirect band gap; (E_F) Fermi energy; (E_{Vb}) valence band.

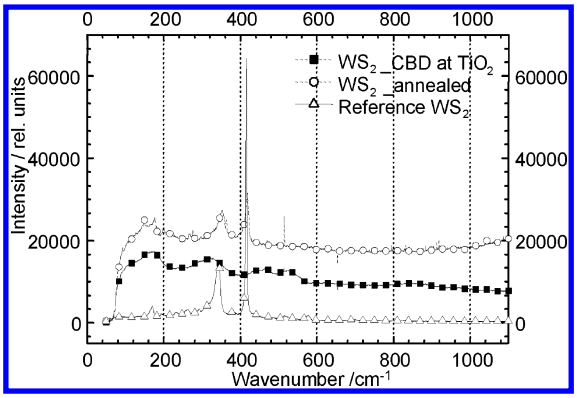

Figure 5. Raman spectrum.

toward the surface of the WS_2 quantum sheet and is injected into the electrolyte (oxidation of iodide to iodine).

On the basis of published energy position data for TiO_2 and WS_2, respectively, an energy diagram can be drawn, which is shown in Figure 4.

Figure 5 shows the Raman spectra of WS_2. The middle spectrum shows the Raman signal obtained from the TiO_2 nanolayer sensitized with WS_2 via CBD. Structures are recognized, but they only partially match the Raman signal obtained from the single crystal (lowest spectrum).

A spectrum similar to the center one (sensitized TiO_2 layer) is obtained when a glass plate is placed in a chemical bath. If such a layer is annealed at 450 °C (which proved to be not feasible with the sensitized TiO_2 layer because of the chemical oxidation of WS_2 in the presence of TiO_2), a Raman spectrum is obtained (top spectrum) which matches the Raman spectrum of WS_2 from single crystals (bottom).

This experiment shows that the chemically deposited WS_2 (without annealing) is present in the form of small and highly disturbed fragments, which assemble into larger crystalline arrays after annealing.

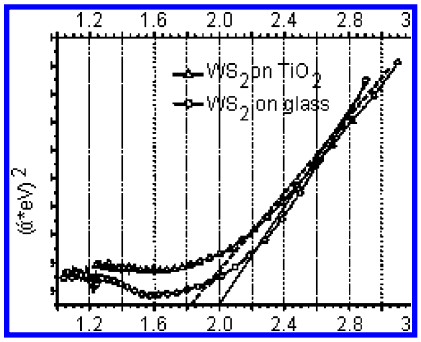

Figure 6. Extrapolation for the determination of the direct band gap.

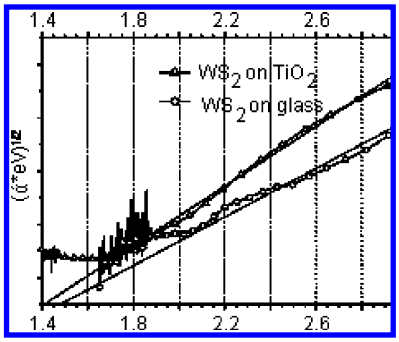

Figure 7. Extrapolation for the determination of the indirect band gap.

Parallel experiments were performed with WSe_2 prepared with an analogue chemical technique. In this case, the Raman pattern obtained with WSe_2 on TiO_2 was much more pronounced and closer to the spectrum observed with WSe_2 crystals. However, no photocurrent was observed. The conduction band of WSe_2 is known to be energetically lower than that of WS_2, which supports our observation.

No TiO_2 Raman spectra have been observed (which have clearly been identified on pure (not sensitized) TiO_2 samples, not shown), which leads to the conclusion that the TiO_2 particles are fully covered and optically interacting with WS_2.

Figures 6 and 7 show $(\alpha h\nu)^{1/2}$ and $(\alpha h\nu)^2$ plots versus energy for the determination of the band gaps from the intercept with the *x*-axis (WS_2 is an indirect gap semiconductor).[11,12]

The indirect band gap can be determined using the following equation:[29]

$$(\alpha h\nu^{1/2}) = k(h\nu - E_g)$$

Here, ά is absorbance, and *k* is a constant. The direct band gap can be determined using the following equation:[20]

$$(\alpha h\nu^{2}) = k(h\nu - E_g)$$

One can observe a slight blue shift between the bulk band gap (1.3 eV[11,12]) and our sample (1.4 eV). We conclude that our particles are so small that quantum size effects occur, and that is why our sample shows a bigger band gap than bulk WS_2. For comparison, absorption of WS_2 on pure glass has been measured. Relative to the band gap energy of bulk WS_2, there seems to be a blue shift in the absorption spectrum. This shift is considered to have been caused by smaller WS_2 crystals in comparison to crystals obtained at TiO_2 and to bulk WS_2.

The results of absorption measurements are summarized in Table 1. When the WS_2 treated TiO_2 nanolayer is exposed to an I^-/I_3^- solution (propylene carbonate) and illuminated, photocurrents are observed. Photocurrent density−voltage de-

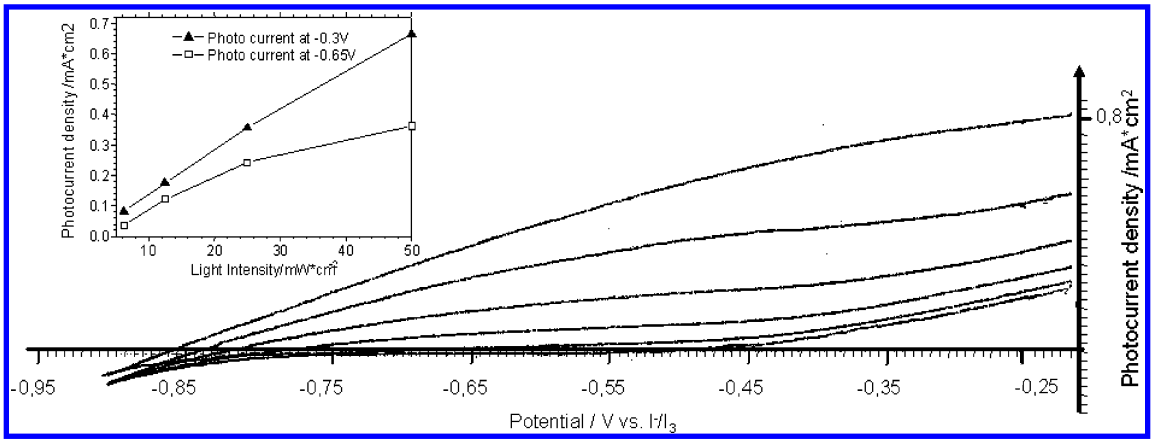

Figure 8. Current−voltage characteristic for different light intensities: (from top to bottom) 50, 25, 12.5, 6.25, 3.1 mW/cm^2, and dark (bottom curve).

TABLE 1

	indirect band gap	direct band gap
bulk WS_2	1.3 eV	1.8 eV
WS_2 on TiO_2	1.4 eV	1.85 eV
WS_2 on glass	1.5 eV	2 eV

pendencies of a TiO_2/WS_2 nanocomposite electrode in contact with propylene carbonate containing 0.5 M LiI are shown in Figure 8 for different light intensities. It is seen that approximately 0.7 mA/cm^2 are reached at a light intensity of approximately 50 mW/cm^2. This photocurrent could already be reached after a chemical reaction time of 2 min for WS_2 deposition. A longer deposition time did not significantly increase the observed photoactivity further. This confirms the finding that due to light excitation WS_2 can generate an excited electron which is transferable into a TiO_2 particle, as to be seen via the photocurrent observed.

It is seen that the current−voltage characteristic does not exhibit an ideal limiting behavior but that the photocurrent gradually increases with the applied voltage (low fill factor). This problem has, in the meanwhile, been addressed and was found to be related to limitations in electron transfer dynamics. As to be shown in a coming contribution, the amino acid cysteine, known from biology as an efficient electron transfer bridge, significantly improves the fill factor of the current voltage characteristic.

The light intensity dependency of the photocurrent for different potentials is shown in the insert. It is seen that some saturation is observed above 25 mW/cm^2.

From single crystals studies of the isocrystalline MoS_2,[30] it is known that the tenside TWEEN 80 (Poly(ethylene glycol) sorbitan monooleate) interacts with and blocks the surface perpendicular to the van der Waals surface. Dark and photocurrents passing this surface are strongly inhibited. Only the more favorable van der Waals surface remains photoactive. Larger photocurrents are observed, because less charge carriers are lost due to recombination at the step sites.

In our case, however, immersing the samples in a 1% aqueous solution of TWEEN 80 resulted in a 30−50% reduction of the photocurrent. This leads to the conclusion that a major part of WS_2 is mediating photoelectrochemical reactions perpendicular to the van der Waals surface.

This means that the nonideal interface of WS_2, which supports higher recombination losses, is involved in the photocurrent turnover.

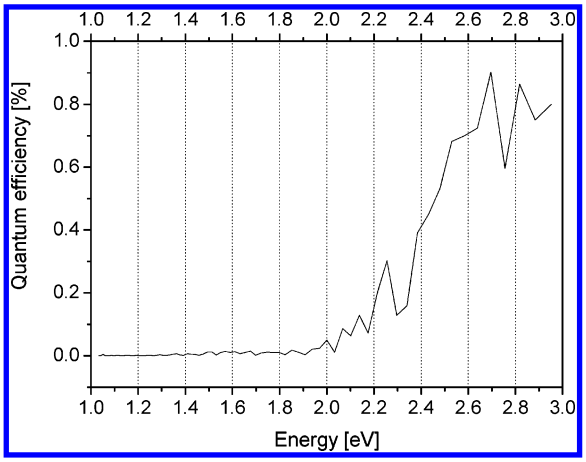

Figure 9. Spectral dependence of the quantum efficiency of nanostructured WS_2 on TiO_2.

How to change this in favor of the more ideal van der Waals surface remains a major challenge for this nanocomposite photoactive material.

The spectrally resolved quantum efficiency of the WS_2 sample in the LiI containing electrolyte is shown in Figure 9. A clear contribution of visible light to the photosensitization of the WS_2 treated TiO_2 nanolayer is observed. The onset of the photocurrent is observed at 1.8 eV, which corresponds to the direct band gap of WS_2 and also agrees with our optical measurements.

To improve the cell efficiency, we have tried to introduce a barrier layer between the TiO_2 particles and the WS_2 cover layer in the nanostructure. Such a layer can influence several factors. First, it can prevent back recombination between TiO_2 electrons and holes from the absorber. Second, it can prevent recombination between TiO_2 electrons and electrolyte or transparent hole conductor (in our case liquid electrolyte). Third, it can change the dipole moments between TiO_2 and the absorber, and the resulting electric field can increase the band offset between them. As a result of the increased band offset, the open circuit voltage will increase. Last but not least, the introduced layer can passivate TiO_2 and may cure surface traps, which are very common recombination centers.

We have tried several materials such as Yt_2O_3, Sc_2O_3, ZnO, Al_2O_3, and MgO. The results are summarized in Table 2. In our case, we have achieved significant improvement of photocurrent with the help of Al_2O_3 coatings. The photocurrent increased 3-fold.

TABLE 2

material	
Yt_2O_3	no effect
ZnO	no effect
Sc_2O_3	no effect
MgO	increase of photocurrent (30%)
Al_2O_3	increase of photocurrent (300%)

Discussion

This study shows that inherently stable layer-type semiconductor particles such as WS_2, the photoelectrochemistry of which is determined by d-states, can successfully be used for sensitized photocurrent generation.

It was demonstrated by Raman spectroscopy that WS_2 is actually produced by chemical reaction. Spectrally resolved electrical measurements as well as band gab extrapolation have confirmed the identity of the absorber material.

Morphological investigations have indicated that the WS_2 absorber nanomaterial is not thicker than 5 nm, and Moiré patterns show that the crystalline structure obtained is not perfect and allows shifts in the stacking of the S−W−S sheets.

Surprisingly, surface passivation experiments using the detergent TWEEN 80, which interacts with the edgy sites of the sheets, indicate that most layers are not growing parallel to the TiO_2 particle surface but perpendicular. This is a drawback because the nonideal perpendicular surface is involved in generating the photoeffects. Ways should be explored to prepare photoactive nanosheets of WS_2 in such a way that the photocurrents are crossing them perpendicular to the van der Waals surface into the electrolyte (or solid contact).

Research on this type of solar energy materials is still in an early stage. A key issue is the separation of electron−hole pairs in an environment with negligible electric fields for charge separation. Molecular electronic mechanisms have to be explored for the improvement rectifiing interfacial properties on the nanoscale.

All together, it may be concluded that the effort toward a nanocomposite solar cell based on stable WS_2 nanoparticles is promising, but several additional challenges including replacement of the electrolyte by a solid-state contact remain to be tackled.

References and Notes

(1) O'Reagan, B.; Grätzel, M. *Nature* **1991**, *353*, 737.

(2) Greijer Agrell, H.; Lindgren, J.; Hagfeldt, A. *Sol. Energy* **2003**, *75* (2), 169−180.

(3) Turrion, M.; Macht, B.; Salvador, P.; Tributsch, H. *Z. Phys. Chem.* (Oldenburg Wissenschaftsverlag, München) **1999**, *212*, 51.

(4) Macht, B.; Turrion, M.; Barkschat, A.; Salvador, P.; Elmer, K.; Tributsch, H. *Sol. Energy Mater. Sol. Cells* **2002**, *73*, 163.

(5) Thomalla, M.; Tributsch, H. IPS 15, Paris, *C. R. Chim.*, submitted.

(6) Liu, D.; Kamat, P. V. *J. Phys. Chem.* **1993**, *97*, 10769−10773.

(7) Shen, Q.; Arae, D.; Toyoda, T. *J. Photochem. Photobiol. A: Chem.* **2004**, *164* (1−3), 75−80.

(8) Underwood, D. F.; Kippeny, T.; Rosenthal, S. J. *J. Phys. Chem. B.* **2001**, *105* (2), 436−443.

(9) Vogel, R.; Hoyer, P.; Weller, H. *J. Phys. Chem.* **1994**, *98*, 3183−3188.

(10) Peter, L. M.; Wijayantha, K. G. U.; Riley, D. J.; Waggett, J. P. *J. Phys. Chem. B* **2003**, *107* (33), 8378−8381.

(11) Nakade, S.; Matsuda, M.; Kambe, S.; Saito, Y.; Kitamura, T.; Sakata, T.; Wada, Y.; Mori, H.; Yanagida, S. *Mater. Chem. Phys.* **2002**, *78*, 234−238.

(12) Ashokkumar, M.; Kudo, A.; Saito, N.; Sakata, T. *Chem. Phys. Lett.* **1994**, *229* (4−5), 383−388.

(13) Thurston, T. R.; Wilcoxon, J. P. *J. Phys. Chem. B* **1999**, *103*, 11−17.

(14) Kline, G.; Kann, K. K.; Ziegler, R. *Sol. Energy Mater.* **1981**, *4*, 301.

(15) Baglio, J. A.; Calabrese, G. S. *J. Electrochem. Soc.* **1982**, *129*, 1461−1472.

(16) Cabrera, C. R.; Abruna, H. D. *J. Electrochem. Soc.* **1988**, *135*, 1436−1442.

(17) Parkinson, B. A.; Furtak, T. E.; Canfield, D. C.; Kam, K.; Kline, G. *Discuss. Faraday Soc.* **1980**, *70*, 233.

(18) Kline, G.; Kam, K.; Parkinson, B. A. *Sol. Energy Mater.* **1981**, *4*, 301−308.

(19) Razzini, G.; Lazzari, M.; Bicelli, L. P.; Levy, F.; De Angelis, L.; Galluzzi, F.; Scafe, E.; Fornarini, L.; Scrosati, B. *J. Power Sources* **1981**, *6*, 371−382.

(20) Tributsch, H. *J. Electrochem. Soc.* **1986**, *133*, 339.

(21) Levy, C.; Tenne, R. Modification of surface properties of layered semiconductors. In *Photoelectrochemistry and Photovoltaics of Layered Semiconductors*; Aruchamy, A., Ed.; Kluwer Academic Publishers: Dordrecht, 1992; Vol. 14, p 155.

(22) Bard, A. J.; Fan, F. *J. Eletrochem. Soc.* **1980**, *128*, 945.

(23) Razzini, G. *J. Power Sources* **1982**, *7*, 275−280.

(24) Bard, A. J.; White, H. S. *J. Electrochem. Soc.* **1982**, *129*, 265.

(25) Djemal, G.; Müller, N. *Sol. Energy Mater.* **1981**, *5*, 403.

(26) Chatzitheodorou, G.; Fiechter, S.; Kunst, M.; Luck, J.; Tributsch, H. *Mater. Res. Bull.* **1988**, *23*, 1261−1271.

(27) Weiss, V. In situ-Untersuchung des Wachstums von reaktiv gesputterten MoSx- und WSx-Schichten mit Hilfe der energiedispersiven Röntgenbeugung (EDXRD). Ph.D. Thesis, FU, Berlin, 2003; pp 157−172 (http://jorge.ub.fu-berlin.de/work/DissSearch).

(28) Reyes-Gasga, J.; Tehuacanero, S.; Jose Yacama, M. *Microsc. Res. Tech.* **1998**, *40*, 2−9.

(29) Pankowe, J. I. Optical Processes in Semiconductors.

(30) Moehl, T.; El Halis, A.; Tributsch, H. *J. Appl. Electrochem.*